

# CrystEngComm

Accepted Manuscript



This is an *Accepted Manuscript*, which has been through the Royal Society of Chemistry peer review process and has been accepted for publication.

*Accepted Manuscripts* are published online shortly after acceptance, before technical editing, formatting and proof reading. Using this free service, authors can make their results available to the community, in citable form, before we publish the edited article. We will replace this *Accepted Manuscript* with the edited and formatted *Advance Article* as soon as it is available.

You can find more information about *Accepted Manuscripts* in the [Information for Authors](#).

Please note that technical editing may introduce minor changes to the text and/or graphics, which may alter content. The journal's standard [Terms & Conditions](#) and the [Ethical guidelines](#) still apply. In no event shall the Royal Society of Chemistry be held responsible for any errors or omissions in this *Accepted Manuscript* or any consequences arising from the use of any information it contains.

# Interplay mechanism of secondary phase particles and the extended dislocations in CdZnTe crystals

Yadong Xu<sup>1,2\*</sup>, Ningbo Jia<sup>1</sup>, Yihui He<sup>1</sup>, Rongrong Guo<sup>1</sup>, Yaxu Gu<sup>1</sup>, Wanqi Jie<sup>1</sup>

1. State Key Laboratory of Solidification Processing, Northwestern Polytechnical University, Xi'an 710072, China

2. Laboratory of Solid State Microstructures, Nanjing University, 210093, China

## Abstract

To interpret the interplay mechanism of dislocations associated with secondary phase (SP) particles,  $\langle 111 \rangle$  CdZnTe crystals are annealed at isothermal and thermal gradient conditions under Cd/Zn and Te overpressure, respectively. Etching pits arrangement surrounding Te-SP is evaluated to give an insight on the generation and multiplication of induced dislocations. It is demonstrated that Te-SP dissociation dominates the volume variation in isothermal annealing. This dissociation is enhanced under Cd/Zn overpressure owing to the exothermic reaction, which results in the activation of dislocations glide and climb systems, simultaneously, the diffusion of Te<sub>i</sub>. In turn, 'radial-shaped' dislocation rosettes and 'star-shaped' dislocation clusters appear on  $\{111\}_B$  surface after preferential etching. However, for thermal gradient annealing, Te-SP thermo-migration is predominated. The induced dislocations density is related with Te droplets drift velocity. While Cd/Zn and Te overpressure could promote or slow the migration. Interestingly, no remarkable dislocation rosettes or clusters are observed after temperature gradient annealing under Te overpressure.

**Keywords:** CdZnTe; Te secondary phase; annealing; dislocation; defect-selective etching

## 1. Introduction

The presence of SP particles often markedly affects the optical and electronic properties of the bulk crystals as well as the surface perfection of epitaxial substrates. They appear not only in II-VI (e.g., CdTe [1], ZnSe [2]), III-V (e.g., GaAs [3]), and IV-VI (e.g., SiC [4]) compounds, but also even in oxides [5] and fluorides [6]. CdZnTe (CZT) crystals have been studied intensively due to their potential applications in X/γ-ray detection and the growth of HgCdTe epilayers [7]. However, local regions with SP particles (inclusions/precipitates) and induced dislocations are usually generated inevitably in as-grown or post-growth annealed CZT crystals [8, 9],

---

\* To whom correspondence should be addressed. Tel: +86-29-88460445. Fax: +86-29-88495414. E-mail address: xyd220@nwpu.edu.cn

which are known to be detrimental to the charge collection of CZT detector [10-12], simultaneously to degrade the epilayers crystallization [13, 14]. Therefore, it is meaningful to study the relationship between SP particles and induced dislocations, in order to tailor bulk crystals with either better performance or lower concentration defects.

Owing to the high melting point of CZT, it is difficult to observe the intricate details of dislocation and SP particle interaction in-situ during growth. Annealing process was considered as an alternative way to evaluate the dislocations associated with SP. Kim *et al.* [15] observed the star-shaped defects with their positions corresponding to those of Te-rich SP particles in CdTe-based compounds after annealing under Cd overpressure, by white-beam X-ray diffraction topography. Sheng *et al.* [16] revealed dislocation multiplication occurred in the regions near Te inclusions after annealing by etching. It was suggested that the characteristic dislocation distribution is attributed to the reaction between in-diffused Cd/Zn atoms and the molten Te inclusions. However, the resulted CdTe and ZnTe compounds possibly prevented the reaction. Besides, the size and pattern of the dislocation clusters varied after different annealing histories. Therefore, to find the driving force that leads to the generation and multiplication of dislocations rosette, the kinetic process of defects interaction should be understood.

To manifest the interplay mechanism between dislocations and Te-SP particles, dislocation arrangement surrounding Te-SP in CZT crystals was investigated after isothermal and thermal gradient annealing under specific atmospheres in this work. By employing defect-selective etching techniques, the distributions of Te-rich SP particles and dislocations on CZT  $\{111\}_B$  face were observed using correlative reflected-light/IR transmission and scanning electron microscopy (SEM). In addition, the extended defects of local areas were identified by transmission electron microscopy (TEM) and cathodoluminescence (CL) microscopy. The mechanism for growth and multiplication of dislocation clusters was proposed on the basis of dissociation-diffusion and thermomigration-deformation. These observations will be helpful to develop CZT post-growth annealing techniques and to correct response non-uniformities of CZT detectors.

## 2. Experimental

$\langle 111 \rangle$ -oriented single crystal wafers with the size of  $10 \times 10 \times 2$  mm<sup>3</sup>, free from twins and grain boundaries, were sliced from detector-grade Cd<sub>0.9</sub>Zn<sub>0.1</sub>Te ingots grown by the modified vertical Bridgman method in our laboratory [17]. Before annealing, the surface damaged layers induced by cutting were removed by lapping,

mechanical and finely chemo-mechanical polish, consecutively. Isothermal and temperature-gradient annealing on CZT wafers were employed under metallic (Cd/Zn) and Te overpressure, respectively, more details are listed in Table 1. However, it is worth mentioning that Te-rich SP particles are significantly affected by both heating and cooling histories. Thus, constant heating rate (100 °C /h) and cooling rate (50 °C /h) were adopted during all the annealing processes.

Everson's solution with the volume ratio of HF, HNO<sub>3</sub> and lactic acid to be 1:4:20 was used to reveal dislocations on {111}<sub>B</sub> face [18]. As a criterion of the dislocation density, etch pit density (EPD) mappings of individual dislocations were created from high-resolution reflected-light microscopy images. The distributions of Te-rich SP particles in bulk crystals were detected by IR transmission microscopy. Te-SP particles and dislocations in selected areas were characterized by correlative reflected-light/IR transmission microscopy and FE-SEM at 15 kV. The extended defects of local areas were identified by CL microscopy and TEM, as detailed in Ref. [9].

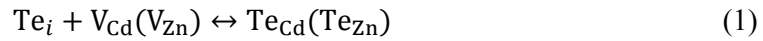
### 3. Results and discussion

To give a convenient comparison, as-grown CZT crystals sliced from the same ingots were utilized, with an average SP particle size approximately of 10~15 μm and a total concentration of (3~4)×10<sup>4</sup> cm<sup>-3</sup> (refer to the Supplementary Data Fig. S1). After etching by Everson solution, the grown-in dislocation density was calculated in the range of (8~9)×10<sup>4</sup> cm<sup>-2</sup> by counting the triangular pyramid etch pits on CZT {111}<sub>B</sub> face. However, dislocations enrichment surrounding Te-rich SP particles was not observed on as-grown CZT surface, as seen in Fig. 1(a).

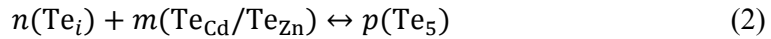
Isothermal annealing was used to adopt to eliminate or reduce Te-SP particles in CZT crystals. But the induced extended dislocations usually appeared. After isothermal annealing at 500 °C under Cd/Zn overpressure, the density of Te-rich SP particles was slightly lower and the average size was reduced, as seen in Fig. S2 in the Supplementary Data. However, the 'radial-shaped' etch pits rosette was usually observed on CZT {111}<sub>B</sub> surrounding Te-SP by defect-selective etching, with typical diameters between 30~60 μm, as seen in Fig. 1(b). The 'radial-shaped' rosette includes six arms radiating from the polyhedral Te-SP at 60° intervals. Unlike the hexagram etching pits rosette on as-grown CZT surface [8, 9], each arm is constituted by a large number of triangular pyramid etch pits. Among which, three inward pyramid etch pits walls are pointing to [211], as indicated by the white dot arrows in Fig. 1(b). Three outward pyramid etch pits walls are pointing to  $[\bar{2}\bar{1}\bar{1}]$ , as indicated by

the red dot arrows in Fig. 1(b). When the isothermal annealing temperature was increased to 650 °C, ‘star-shaped’ dislocation clusters with size in the range 200~300 μm were emerged without the Te-SP, as seen in Fig. 1(c), which comprised by plenty of pyramid etch pits, as Fig. 1(d).

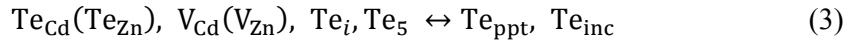
Due to CZT crystal grown under Te-rich condition, Te interstitials ( $Te_i$ ) appear as the main grown-in point defects in the view of Te saturation at high temperature. However, the highly mobile  $Te_i$  diffuse through the crystal to highly prevalent the cation vacancies ( $V_{Cd}/V_{Zn}$ ) and generate immobile Te anti-sites during the in-situ annealing and slow cooling-down process according to the defect reactions [19, 20],



Te anti-sites attract additional  $Te_i$ , forming the Te-rich cluster of 5Te atoms in a triangular arrangement [21].



Certainly, partial of native point defects and  $Te_5$  clusters tend to escape into Te-rich SP particles (Te precipitate  $Te_{ppt}$  or Te inclusion  $Te_{inc}$ ) or to get together.



On the contrary, when annealing above the melting point of Te (>450 °C), the dissociation of Te-rich SP particle becomes active, accompanied by an increase of the  $Te_i$  concentration around Te-SP according to Eq. 1~ Eq. 3.

A mechanistic pathway of dissolution-diffusion based on isothermal annealing under Cd/Zn overpressure is proposed as schematized in Fig. 2. First the local deformation occurred due to Te-SP melting and dissociating, which results in the release of stress into CZT matrix. The stresses in a grain may depend on the orientation of the surrounding facets. In that Te-SP is covered by  $\{111\}_{CZT}$  and  $\{100\}_{CZT}$  facets [22], the lattice glides by tensile stress and compressive stress are propagated along  $\langle 111 \rangle$  and  $\langle 100 \rangle$  directions, respectively. Then dislocations line up and parallel to the traces of the corresponding loop planes. The projections of these loop planes on  $\{111\}$  surfaces coincide  $\langle 211 \rangle$ , which is inclined to each other at 60°, as indicated by the blue and red dot arrows shown in Fig. 2, thus giving the characteristic ‘radial-shaped’ feature. Further,  $Te_i$  will diffuse into the specimen since the concentration gradient, with the direction is likely consistent with the way of dislocation loop punching. It was demonstrated by the dark dots in the panchromatic CL image of Te-SP on CZT  $\{111\}_B$  face, as seen in Fig. S3 in the Supplementary Data.

Te<sub>i</sub>-related defects are suggested to be responsible for the non-radiative recombination process at the dislocation-rich region.

The dissociation of Te-SP is largely related to the solubility of Te<sub>i</sub>, which is depended on the temperature. The mean dimension of the etch pits rosettes on {111}<sub>B</sub> after isothermal annealing is plotted in Fig. 3. Owing to the dislocation climb systems were enhanced by the point defects [23], the resulted dislocation walls extended by the diffusion of Te<sub>i</sub>. As well know, in the given annealing time (*t*), the effective diffusion distance (*d*) of Te<sub>i</sub> is proportional to  $\sqrt{Dt}$ . *D* is the diffusion coefficient, which can be expressed by an Arrhenius equation [24],

$$D = D_0 \exp\left(-\frac{Q}{RT}\right) \quad (4)$$

where *D*<sub>0</sub> is the diffusion constant, *R* is the ideal gas constant, and *T* is the temperature, *Q* is the diffusion activation energy (J·mol<sup>-1</sup>). By fitting the linear plot of ln *D* versus 1000/*T*, the activation energy with the value approximately of 39 kJ·mol<sup>-1</sup> (0.4 eV) is obtained, which is consistent with Ref. [23]. It was ascertained that in the given annealing time the dislocations enriched region was exponentially increased as temperature rising. Simultaneously, it was also demonstrated by the shrinkage of the polyhedral core, as shown in Fig. 2 I-III.

On the other hand, since the annealing was adopted under metallic overpressure, Cd and Zn atoms tended to diffuse into CZT bulk within the given time [25]. The exothermic reaction between Cd/Zn and Te<sub>i</sub> happened.



Due to low thermal conductivity, heat ( $\Delta E$ ) can not be dispersed in time, in turn the dislocations glide/climb intensified by the thermal stress ( $\sigma_T$ ) in CZT matrix. When many slip systems activated simultaneously by  $\sigma_T$  because of a more favorable orientation, 'star-shaped' pyramid etch pit clusters were generated, as seen in Fig. 2-IV.

In the case of isothermal annealing under Te overpressure, the density of Te-SP particles was slightly lower, but the average size was enlarged, as seen in Fig. S2 in the Supplementary Data. Neither 'radial-shaped' nor 'star-shaped' dislocations clusters are observed on {111}<sub>B</sub> face after defect-selective etching, as shown in Fig. S4 in the Supplementary Data. Although the dissociation dominates the volume variation of Te-SP, the diffusion of Te<sub>i</sub> is limited by the saturated Te overpressure. Besides, due to no exothermic reaction occurs during annealing, dislocations glide

driven by  $\sigma_T$  is not activated. Finally, the well-defined polyhedral Te-SP particles were expanded by the aggregation of Te related point defects, which is in agreement with the IR image statistic. In addition, the riping of Te-SP has also been recognized according to the aggregation of nano-size Te precipitates by revealing a cross-sectional view of Te-SP using FIB technique (refer to Supplementary Data). The coherent and incoherent Te precipitates were observed surrounding Te inclusions. However, it should be noted that there is temperature gradient between CZT bulk and the surface even under isothermal situation at both heating and cooling procedure, due to its low thermal conductivity.

Except isothermal annealing, annealing under a temperature gradient field can drive Te-SP droplets to migrate, in turn to reduce Te-SP density, owing to the temperature gradient zone melting (TGZM) mechanism [26]. However, the induced dislocations distribution is different.

In respect of the annealing under metallic overpressure at 650/550°C (CZT/Cd-Zn), large-size Te-SP particles are significantly eliminated, only small dark dots with size of 5-10  $\mu\text{m}$  present in IR image, as seen in Fig. S2 in the Supplementary Data. After defect-selective etching, numerous triangular pyramid etch pits on CZT  $\{111\}_B$  surface are observed, with the cavities caused by Te-SP evaporation under Cd/Zn overpressure, as shown in Fig. 4(a). To give an evaluation in depth, the surface layer of  $\sim 0.1$  mm was firstly removed on CZT  $\{111\}_B$ . Both ‘radial-shaped’ etch pits rosette and ‘star-shaped’ etch pits clusters can be found in Fig. 4(c). Until 0.25 mm layer polished off, uniform dislocations distribution appears, however, with the density is twice more than that in as-grown CZT, as shown in Fig. 4(b).

According to our previous study [27], the thermomigration-deformation is predominated based on the melt-recrystallization theory, as seen in Fig. 4(d). The well-defined polyhedral Te-SP particles tend to melt and migrate toward the hot sides due to the temperature gradient. The steady drift velocity of droplets  $v$  under such conditions can be described as

$$v = \frac{D_{CZT}}{c_S} \nabla T \left( \frac{dc}{dT} + S_T c_L \right) \quad (6)$$

where  $c_S$  and  $c_L$  are the solute concentration in the solid and liquid, respectively,  $D_{CZT}$  is the diffusion coefficient of CZT in Te droplet,  $\nabla T$  represents the temperature gradient of the wafer,  $S_T$  is the Soret coefficient of CdTe-Te solution system.  $dc/dT$  is

approximately equal to the reciprocal of liquidus slope on Te-rich side of the CdTe-Te phase diagram.

Plastic deformation of Te-SP particle is accompanied by the shape change and merging during the migration, as seen in Fig. 5(a) the typical quenched sample. However, the void is difficult to move, which used to be left in CZT bulk. Owing to the scattering effect, the void with size smaller than Te-SP usually has dark contrast in IR images. To further certify, SEM images was obtained on CZT surface after removing 0.25 mm surface layer. EDS mappings demonstrate that neither Te nor Cd element in the dark dot, as shown in Fig. 5(b) and (c).

The recrystallization quality is related with the drift velocity of Te droplets. Severe lattice misfit could be happened in the near surface region due to higher  $v$ . Meanwhile, part of the Te-SP dissociated, which resulted in the similar dislocation etching pits rosette. In addition, a higher number of active dislocations tended to move to the surface due to the image force. Dislocation multiplication was also promoted by the misfit stress resulted by the local composition fluctuation. Therefore, although the large-size Te-SP particles are eliminated, the dislocations density in the bulk is increased after temperature-gradient annealing under metallic overpressure.

Generally, the source temperature should be lower than that of CZT wafers during annealing. However, to avoid the effect of surface evaporation, temperature-gradient annealing under Te overpressure was utilized at 650/750°C (CZT/Te). Tellurium sources were inclined to deposit on CZT surface after annealing. Surface layer of  $\sim 0.1$  mm was removed prior to IR image, both size and density of Te-SP particles reduced, as seen in Fig. S2 in the Supplementary Data. But, interestingly, no remarkable dislocations rosettes and clusters were observed on  $\{111\}_B$  face after defect-selective etching. When 0.25 mm layer was polished off, dislocations density was found similar to that in as-grown CZT.

Actually, the Te concentration gradient and the real temperature gradient  $\nabla T$  in CZT wafer could be degraded by the deposited Te source. According to Eq. (6), Te-SP migration velocity  $v$  was reduced. Therefore, the dislocations glide and climb by lattice deformation were possibly relaxed during melt-recrystallization [28]. Besides, thermal stress induced dislocations were not significant due to no exothermic reaction occurred during annealing.

#### 4. Conclusions

In summary, the size and distribution of Te-rich SP particles and the induced dislocations in CZT crystals were evaluated before and after the annealing under different situations. Our investigations demonstrated that Te-rich SP particles were more efficiently eliminated under thermal gradient annealing than that under isothermal annealing in the given time. However, the ‘radial-shaped’ dislocation rosettes and ‘star-shaped’ dislocation clusters were observed more frequently after annealing under Cd/Zn atmosphere. The driving forces that lead to the generation and multiplication of the dislocation rosettes have been discussed.

During the isothermal annealing at Cd/Zn overpressure, Te-SP dissociation dominates the volume variation, which results in the dislocations glide and climb systems activate, simultaneously with the diffusion of  $Te_i$ . Then growth and multiplication of the dislocations are enhanced by the local thermal stress, which is attributed to the exothermic reaction between Cd/Zn and  $Te_i$ . However, for the thermal gradient annealing, Te-SP migration towards the high temperature side is superior to its dissociation. The induced dislocations density is related with the drift velocity of Te droplets. But the Te-SP migration could be possibly promoted or slowed by the Cd/Zn and Te overpressure, respectively. In addition, our results demonstrate great potential for understanding of SP-particles associated dislocations in other bulk materials.

### Acknowledgements

This work has been financially supported by National Natural Science Foundations of China (51202197 and 51372205) and the National “973” Program (2011CB610406). It is also supported by the Specialized Research Fund for the Doctoral Program of Higher Education of China (20116102120014), and the Natural Science Basic Research Plan in Shaanxi Province of China (2014K06-13).

### References

- [1] P. Rudolph, A. Engel, I. Schentke, A. Grochocki, *J. Cryst. Growth*, 1995, **147**, 297-304.
- [2] P. Rudolph, N. Schäfer, T. Fukuda, *Mater. Sci. Eng. R.* 1995, **15**, 85-133.
- [3] S. Eichler, W. Fliegel, M. Jurisch, A. Kohler, M. Naumann, A. Rockoff, *J. Cryst. Growth*, 2008, **310**, 1410-1417.
- [4] R. Han, X. Xu, X. Hu, N. Yu, J. Wang, Y. Tian, W. Huang, *Optical Materials*, 2003, **23**, 415-420.

- [5] P. Fiorenza, V. Raineri, S. Ebbinghaus and R. Nigro, *Crystengcomm*, 2011, **13**, 3900-3904.
- [6] L. Su, Y. Dong, W. Yang, T. Sun, Q. Wang, J. Xu, G. Zhao, *Mater. Res. Bull.*, 2005, **40**, 619-628.
- [7] T. E. Schlesinger, J. E. Toney, H. Yoon, E. Y. Lee, B. A. Brunett, L. Franks, and R. B. James, *Mater. Sci. Eng. R.* 2001, **32**, 103-189.
- [8] Y. Xu, Y. He, T. Wang, R. Guo, W. Jie, P. Sellin and M. Veale, *Crystengcomm*, 2012, **14**, 417-420.
- [9] Y. He, W. Jie, Y. Xu, Y. Wang, Y. Zhou, H. Liu, T. Wang, G. Zha, *Scripta Materialia*. 2014, **82**, 17-20.
- [10] G. A. Carini, A. E. Bolotnikov, G. S. Camarda, G. W. Wright, R. B. James, and L. Li, *Appl. Phys. Lett.* 2006, **88**, 143515.
- [11] E. S. Elshazly and G. Tepper, *Appl. Phys. Lett.* 2008, **93**, 042112.
- [12] A. Hossain, A. Bolotnikov, G. Camarda, R. Gul, K. Kim, Y. Cui, G. Yang, L. Xu and R. James, *J. Appl. Phys.* 2011, **109**, 044504.
- [13] S. Sen, C.S. Liang, D.R. Rhiger, J.E. Stannard, and H.F. Arlinghaus, *J. Electron. Mater.* 1996, **25**, 1188-1195.
- [14] F. Sheng, C. Zhou, S. Sun, and J. Yang, *J. Electron. Mater.* 2014, **43**, 1398-1402.
- [15] K. Kim, A. Bolotnikov, G. Camarda, J. Franc, P. Fochuk, R. James, *J. Cryst. Growth*, 2014, **390**, 1-4.
- [16] F. Sheng, J. Yang, S. Sun, C. Zhou and H. Yu, *J. Electron. Mater.* 2014, **43**, 2702-2708.
- [17] Y. Xu, W. Jie, P. J. Sellin, T. Wang, L. Fu, G. Zha, P. Veeramani, *IEEE Trans. Nucl. Sci.* 2009, **56**, 2808-2813.
- [18] P. D. Brown, K. Durose, G. J. Russell and J. Woods, *J. Cryst. Growth*. 1990, **101**, 211-215.
- [19] R. Grill, J. Franc, P. Hoschl, I. Turkevych, E. Belas, P. Moravec, M. Fiederle, and K. W. Benz, *IEEE Tran. Nucl. Sci.*, 2002, **49**, 1270-1274.
- [20] D. Hurle, *J. Appl. Phys.* 1999, **85**, 6957-7022.
- [21] V. Lordi, *J. Cryst. Growth*, 2013, **379**, 84-92.
- [22] Y. He, W. Jie, Y. Xu, T. Wang, G. Zha, P. Yu, X. Zheng, Y. Zhou, H. Liu, *Scripta Materialia*, 2012, **67**, 5-8.
- [23] X. Zhou, D. Ward, B. Wong, F. Doty, and J. Zimmerman, *The Journal of Physical Chemistry C*, 2012, **116**, 17563-17571.
- [24] K. Huang, X. Xie, Semiconductor Physics, Beijing, 1958, (in Chinese, Chapters 1-3).
- [25] T. Lee, J. Park, Y. Jeoung, H. Kim, C. Chun, J. Kim, I. Park J. Chang, S. Kim, M. Park, *J. Electron. Mater.* 1995, **24**, 1053-1056.

- [26] T. Anthony, H. Cline, Thermal Migration of Liquid Droplets through Solids, *J. Appl. Phys.* 1971, **42**, 3380-3387.
- [27] Y. He, W. Jie, T. Wang, Y. Xu, Y. Zhou, Y. Zaman, G. Zha, *J. Cryst. Growth*, 2014, **402**, 15-21.
- [28] A. Zappettini, N. Zambelli, G. Benassi, D. Calestani, and M. Pavesi, *Appl. Phys. Lett.* 2014, **104**, 252105.

Table 1 Annealing parameters for CZT crystals under different situations.

Annealing	Atmosphere	$T_{\text{wafers}}$ (°C)	$T_{\text{sources}}$ (°C)	$\nabla T^*$ (°C/cm)	Annealing time $t$ (h)	Processing label
Isothermal	Cd/Zn overpressure	500-700		-	60	Ann-1
	Te overpressure	500-700		-	60	Ann-2
Temperature-gradient	Cd/Zn overpressure	650	550	7-8	60	Ann-3
	Te overpressure	650	750	7-8	60	Ann-4

\* $\nabla T$  represents the temperature gradient of wafers during annealing.

### Figure Captions

Fig. 1 (a) SEM image of as-grown CZT  $\{111\}_B$  face after etching by Everson solution. (b) ‘Radial-shaped’ etch pits rosette surrounding a Te-SP. (c) Typical optical image of CZT  $\{111\}_B$  by defect-selective etching after 650 °C Ann-1 annealing. (d) ‘Star-shaped’ dislocation cluster.

Fig. 2 Diagram of the evolution of Te-SP and the surrounding etch pits rosette on CZT  $\{111\}_B$ . From left to right, the temperature increases.

Fig. 3 The mean diameter of the etch pits rosette as a function of  $1000/T$ , with the measurement error of  $\pm 3\%$ . The red line is the linear fitting result.

Fig. 4 (a) The cavity caused by Te SP separation. (b) 0.25 mm layer was removed, (c) 0.1 mm layer was removed, insert are the enlarged pits clusters. (d) A diagram of thermomigration-deformation.

Fig. 5 (a) Typical IR images of as-grown CZT crystals and after 2 h, 10 h annealing. (b) SEM image on CZT crystal after 60 h temperature-gradient annealing with 0.25 mm layer removed. (c) Enlarged void and the corresponding Te ( $L\alpha$ ), Cd ( $L\alpha$ ) peak mappings derived from EDS spectra.

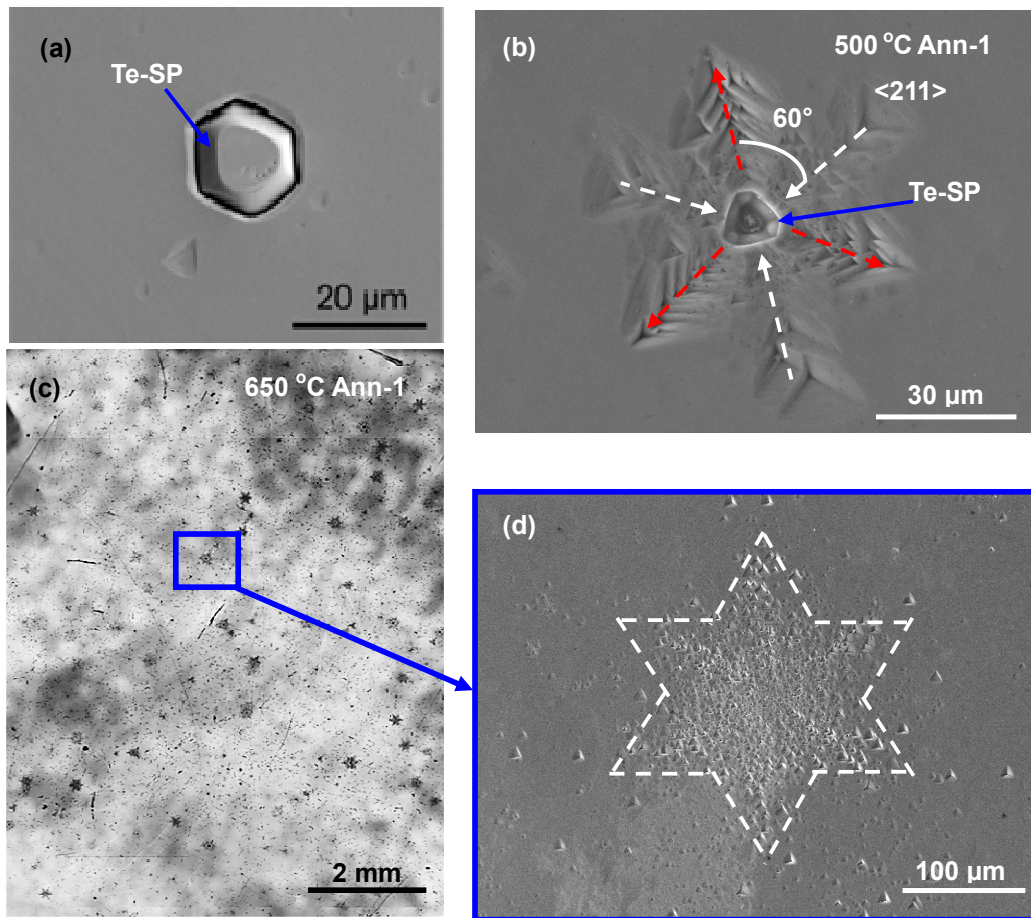


Fig. 1

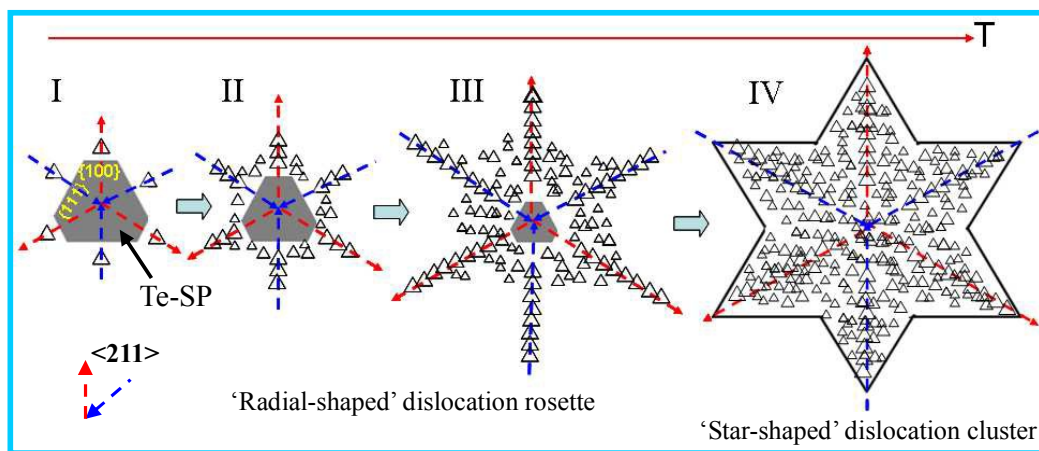


Fig. 2

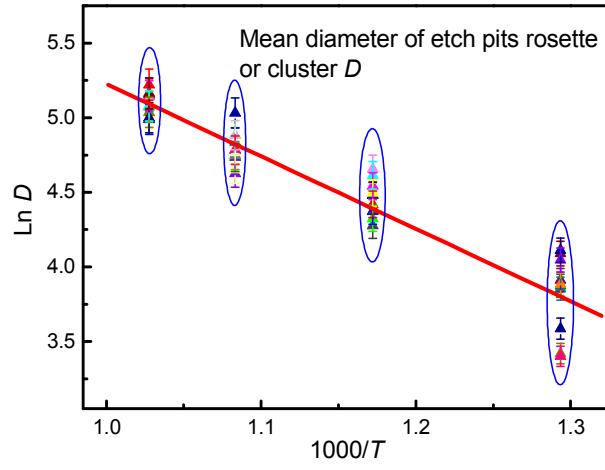


Fig. 3

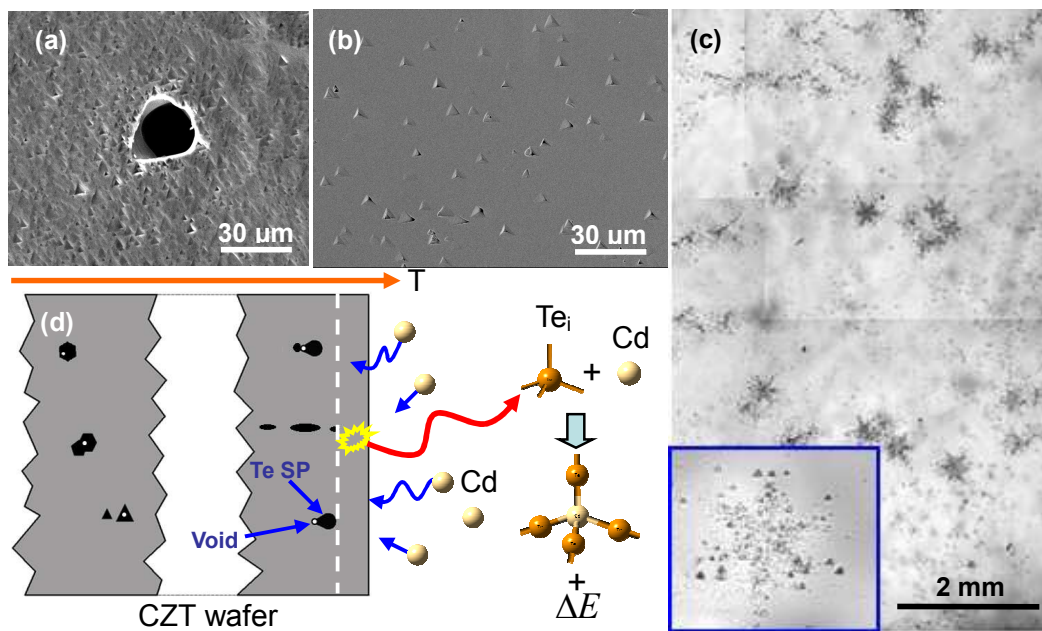


Fig. 4

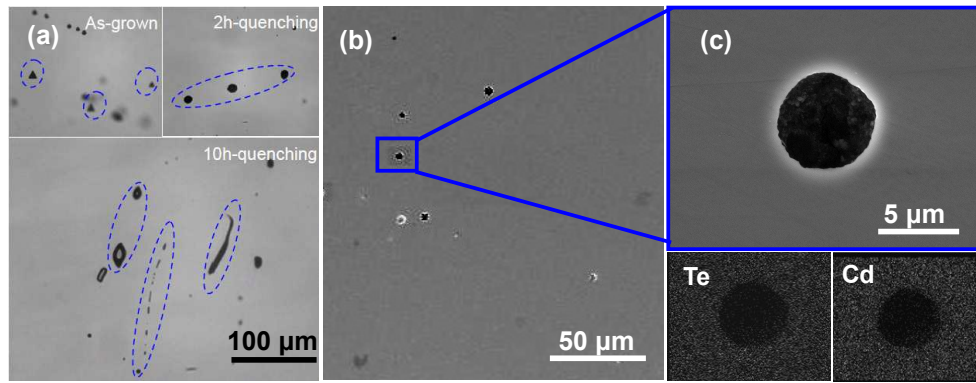


Fig. 5

Te-rich secondary phase dissociation dominates the volume variation during isothermal annealing, which results in the activation of dislocations glide and climb systems, simultaneously, the diffusion of Te interstitials ( $Te_i$ ).

